AIAA AVIATION Forum
June 27-July 1, 2022, Chicago, IL & Virtual
AIAA AVIATION 2022 Forum

10.2514/6.2022-4136

Unsteadiness in Shock/Boundary-Layer Interaction Over a Compliant Panel at Mach 2

Mustafa N. Musta[1], Yoo-Jin Ahn[2], Marc A. Eitner[3], Jayant Sirohi[4], and Noel T. Clemens[5]
Department of Aerospace Engineering and Engineering Mechanics, The University of Texas at Austin, Austin, TX, 78712, USA

This work investigates surface pressure unsteadiness on a compliant panel under a shockwave/boundary-layer interaction (SBLI) induced by a 2D compression ramp with an angle of 20º in a Mach 2 wind tunnel. High-speed digital image correlation (DIC) and fast-response pressure-sensitive paint (PSP) measurements are used to measure the panel displacement and panel and ramp-face surface pressure fluctuations at 5kHz and 20kHz, respectively. The data reduction technique of POD (proper orthogonal decomposition) was employed both for pressure and displacement fields. POD mode distribution for the pressure fields reveals that the first six modes have 60% of the total energy and exhibit low-frequency content for both rigid and compliant panels. The vibration of the compliant panel was seen to alter the energy distribution of the high energy modes as compared to the rigid panel case. The cross-correlations between the displacement and pressure modes were made using the time coefficients. This analysis shows significant correlations were present among the lower modes. The highest correlation was between displacement mode 1 and the pressure mode 4, which stemmed from the upstream of the intermittent region. The analysis was also made for the surrogate shock foot and reattachment lines. The correlation shows that panel vibration lowers the correlation between the shock foot and reattachment line when compared with the rigid panel case.

δ_{99}	=	Boundary layer velocity height based on 99% free stream.
U_{BL}	=	Boundary-layer edge velocity
U_{∞}	=	Freestream velocity
Re	=	Reynolds number
x	=	Streamwise coordinate
y	=	Wall-normal coordinate

I. Introduction

Supersonic and hypersonic vehicles are subjected to strong pressure fluctuations and thermal loading linked to unsteadiness associated with shock/boundary layer interactions (SBLIs). SBLIs occur on numerous locations over a vehicle including in inlets and engines, wing roots, fins, divert jets and other control surfaces. Strongly separated interactions typically exhibit low-frequency broadband unsteadiness that generally is one to two orders of magnitude lower than the characteristic boundary layer frequency [1], [2] . High-speed vehicles are often thin-wall structures that become compliant in the presence of aerothermo heating, and thus can dynamically-respond to the low-frequency pressure fluctuations associated with SBLIs. The excited structural resonant modes can lead to rapid fatigue and failure

[1] Lecturer, Member
[2] Graduate Student, Member
[3] Postdoc, Member
[4] Professor, Associate Fellow
[5] Professor, Fellow

of such compliant structures [3]Several studies have examined FSIs resulting from SBLIs occurring due to reflected shocks. Some studies have found that the mean loading on a thin structure affects the flow dynamics [4], and the flow-structure interaction affects shock foot frequency [5]. Studies by Spottswood et al. [6]–[8] demonstrate coupling at lower frequencies between panel displacement and surface pressure fields. Further experimental studies of the last decade can be found in the literature ([9]–[13]).

Previous work by the current authors have examined the FSI generated by a Mach 2 two-dimensional compression ramp located at the aft-end of a compliant panel using simultaneous high-speed DIC and PSP [14]–[17][18], [19]. Measurements were made on both polycarbonate and brass thin panels. The latter was studied to avoid possible visoelastic effects that could be present with the polycarbonate panels. For the polycarbonate panel studies, results showed a strong correlation between displacement and pressure for the fundamental mode, and there is evidence that the shock foot motion becomes “locked in” to the first mode oscillations. Studies with brass panels of thickness h=0.010"-0.020" revealed that the linearized potential flow theory holds upstream of the separation shock and the gradient of the surface deformations (i.e., wall angle) can be used to predict the pressure fluctuations. It was also found that the second vibrational mode shape was affected by the shock-foot motion but not the first mode[19] i.e., only the second mode showed a two-way coupling effect.

Further measurements on the 1 mm polycarbonate compliant panel, including the ramp surface, revealed that the compliant-panel-induced low-frequency unsteadiness persisted even on the face of the rigid ramp. There is also a correlation at the reattachment as well. Additionally, the spectral POD method and bandpass filtering around the structural modes agreed well on the nature of the displacement and pressure field mode shapes [[20].

The current work focuses on the unsteadiness of the 1 mm thick polycarbonate panel under the same Mach 2 compression ramp SBLI. The rigid panel fast response pressure measurements were used as a baseline for comparison, and POD analyses were made on the pressure field. The coupling between the displacement and pressure modes was investigated. Surrogate shock foot and reattachment line correlations were also analyzed for the rigid and the compliant panel.

A. Facility and Set-Up

Mach 2 blow-down wind tunnel facility at The University of Texas at Austin was utilized. The facility provides a free stream velocity of 514 ± 3.8 ms^{-1}, stagnation conditions of 345 ± 5 kPa and 292±5 K, and a nominal run time of 30 seconds. The free stream and wall condition Reynolds numbers are Re_∞=3.8×10^{7} m^{-1} and Re_w=4.67×10^{5} m^{-1}, respectively, and the freestream turbulence intensity is less than 1%. The compressible momentum (θ) and displacement (δ^*) thicknesses are 0.9 mm and 2.6 mm, respectively, and Re_θ~ 34,200 [21], [22].

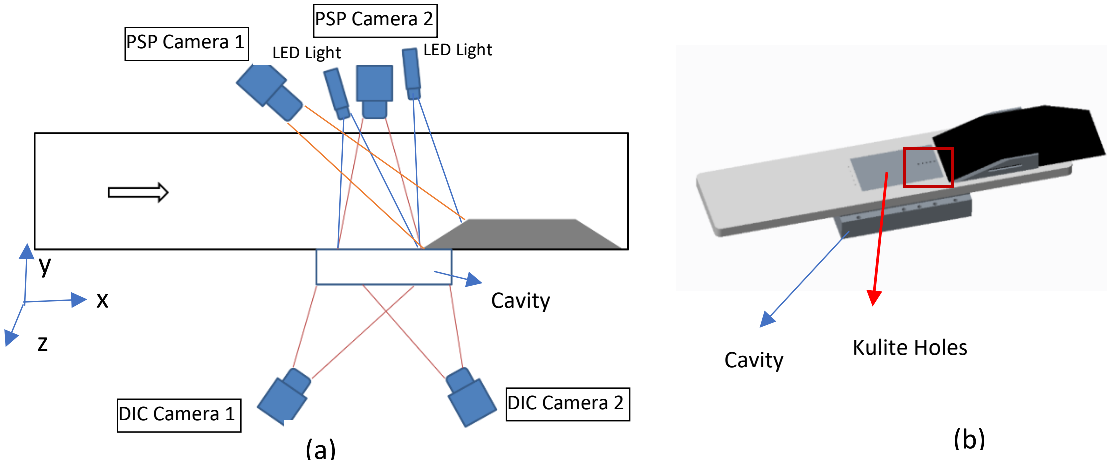

Figure 1 (a)2D view of Experimental Set-Up for simultaneous PSP and DIC. b) Schematic of compression ramp with the rigid panel, tunnel floor, and cavity.

The 20° compression ramp was centered in the wind tunnel with fences that extend 10 mm upstream of the ramp (Figure 1 b). A floor plug section facilitates installation of either a rigid panel or a thin compliant panel, which was placed immediately upstream of the ramp. A sealed window cavity was fitted below the compliant panel to allow arbitrary selection of the panel backpressure. For this experiment, it was measured at 6.4 ± 0.1psi. The windowed cavity allows an unobstructed view of the back surface of the compliant panel for DIC. The compliant panel was made from polycarbonate, 127 x 68.5 mm, with thicknesses of 1 mm. The material and thickness of the compliant panel were selected 1 mm to give the desired set of low modal frequencies of 351 Hz, 473 Hz, and 675 Hz, that were calculated using analytical relations from Blevins & Plunkett [23]. Impact testing was performed to experimentally obtain the modal frequencies for the first mode, which was measured to be 407 Hz. Several spanwise pressure transducers can be placed into the upstream section of the panel. The rigid panel provided a baseline case for pressure measurements and features pressure transducer locations at the upstream edge and along the mid-line near the ramp junction.

High-speed discrete surface pressure measurements were made for in-situ calibrations of the PSP, and the PSP dynamic response was assessed at seven streamwise pressure transducer locations. Five of them were with a 3 mm pitch along the midline of the tunnel near the ramp junction (Figure 1b). These transducers were placed throughout the separation region, which features high-frequency, high-amplitude unsteadiness and a wide range of pressures that are good for both calibrating and assessing the temporal response of the PSP. For the compliant panel features, the transducers that were located just upstream of the panel, and thus in the undisturbed boundary layer, were used for in-situ calibration to obtain tunnel static pressure during each run. The pressure transducers used in this study are ultra-miniature Kulite transducers (XCQ-062-50) and have a temporal response of approximately 50 kHz, as given by the manufacturer. The pressure transducers were calibrated at least once per day. A NIMax PXIe 1030 DAQ with two PXIe-4331 modules recorded the pressures from the transducers at 140 kHz and filtered the signal to 100 kHz. The total uncertainty of the pressure measurements is around 2% of the wall static pressure (~700 Pa), assessed by summing the component uncertainties according to a root-sum-of-squares law [24].

The polymer/ceramic pressure-sensitive paint (PC-PSP) was used for high-speed pressure measurements. The PSP uses a ruthenium luminophore ((Ru)ddp3), a silicon rubber binder, TiO2 base, and toluene solvent with a recipe of (Ru)ddp3 (15mg) + TiO2 (92%wt) + Silicone (8%wt) +(Toluene (9ml)+dichloromethan (6ml) [25]. PSP images were recorded at 20 Hz using FastCam Mini, and Nova S with two in-house LED light sources (Figure 1a). The total number of images acquired per experiment is 32000, limited by the camera memory. The panel was imaged fully with a resolution of 352x624 pixels (PSP Camera 1 in Figure 1a), and on the ramp over a 68.5mm x 68.5mm area, it was acquired by 512x512 pixels. The light sources emit at 450 ± 10 nm with a high-pass filter that removes content above 550 nm. The camera is also low-pass filtered (650 nm cutoff) to render the paint emission detectable.

The PSP paint calibration was calculated in-situ using the pressure transducers. The calibration is achieved by comparing the run averaged pressure transducer measurements to the run averaged 'virtual transducers' that are extracted from the PSP at locations adjacent to the Kulites. Calibration results showed good agreement of PSP compared to Kulites measurement on the panel up to 10khz [20]

Stereoscopic digital image correlation (DIC) allows assessing the 3D surface deformation of the compliant panel. The DIC system uses two high-speed cameras (labeled DIC Cameras 1&2 in Figure 1) to obtain full three-dimensional displacement fields of the panel surface. The DIC cameras (Phantom Miro M310) are mounted under the tunnel and recorded 10000 images at 5kHz. A random speckle pattern is applied to the lower side of the compliant panel, which the system views from under the tunnel through the windowed cavity. All DIC images have been processed using LaVision DaVis v10 by setting an interrogation window size of 19x19 pixels with a 7-pixel overlap.

B. Pressure field measurement and spectral content

In order to show the characteristics of the pressure field, Figure 2 shows sample surface pressure fields on the compliant panel and ramp. The panel and ramp conjunction is at x/δ_{99}= 0 and negative distances are upstream of the ramp corner. Interpretation of the PSP (Figure 2) is as follows: the blue is the free stream, the aqua/green is the shock foot, the yellow/orange is the separation region, and yellow/red is the reattachment. The sequence images show that the region between the surrogate shock-foot and reattachment line varies over time Figure 2(a-c). A careful look at the upstream region -10< x/δ_{99}= < -3.5 wavy spanwise patterns are believed to be Mach-waves generated by upstream-located wind tunnel wall junctions. The darker blue contours in the same section are due to the panel deformation.

The streamwise evolution of the spectral content of the compliant panel is shown on Figure 3. The midline of the compliant panel z/δ_{99}~0 was chosen to compare the streamwise evolution of spectral content. For each streamwise location, pre-multiplied PSD of pressure was calculated $(f \cdot G(f))$ and normalized by the variance. Figure 3(a,b) shows a spectral peak at about 360-400 Hz along the length of the panel, which even continues onto the ramp face. This frequency is close to the first natural frequency of the panel. The figure shows that the highest peak is at the highest amplitude of the first mode. In the intermittent region where shock-foot oscillates, the lower frequency content dominates due to the lowpass filtering effect of the shock foot (x/δ_{99}= ~-2.9 and Figure 3a green plot). On that line, the peak frequency is at ~400Hz and so it appears that the panel natural frequency affects the shock-foot dynamics.

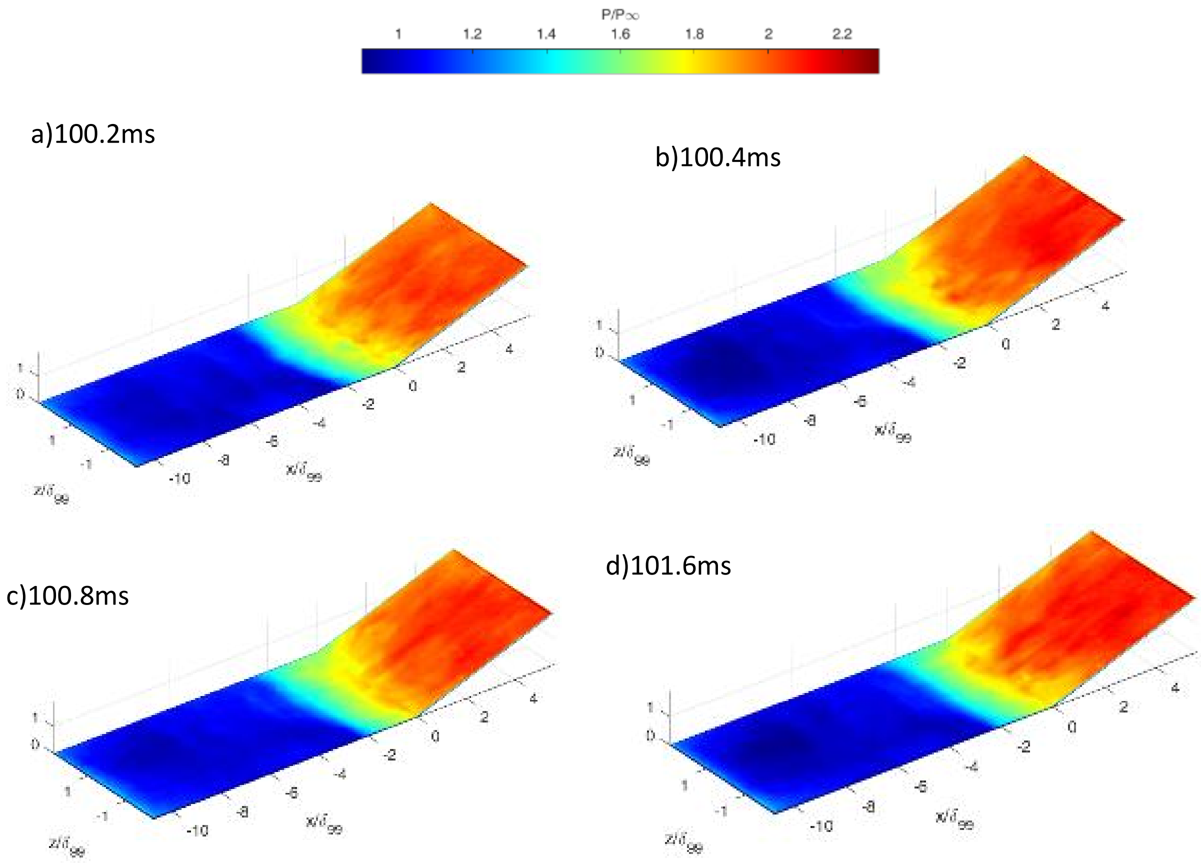

Figure 2 Snapshots from pressure fields for the compliant panel case

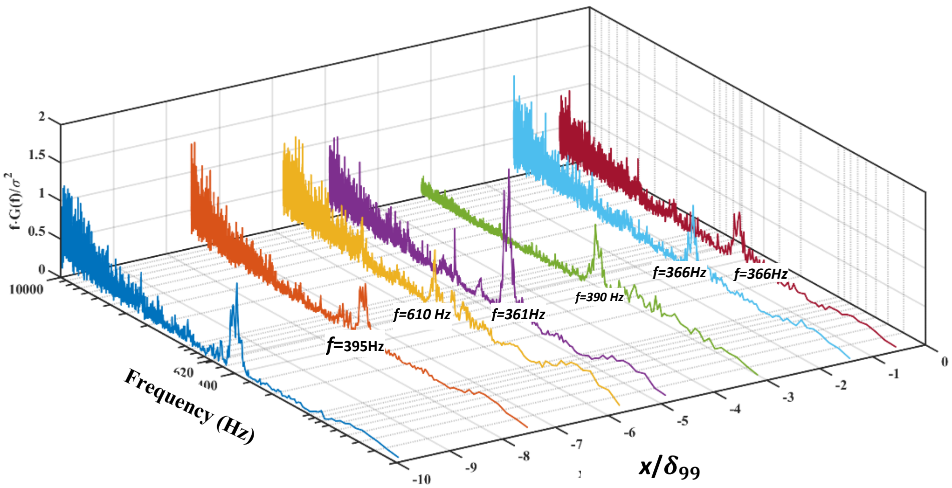

a) Panel Surface

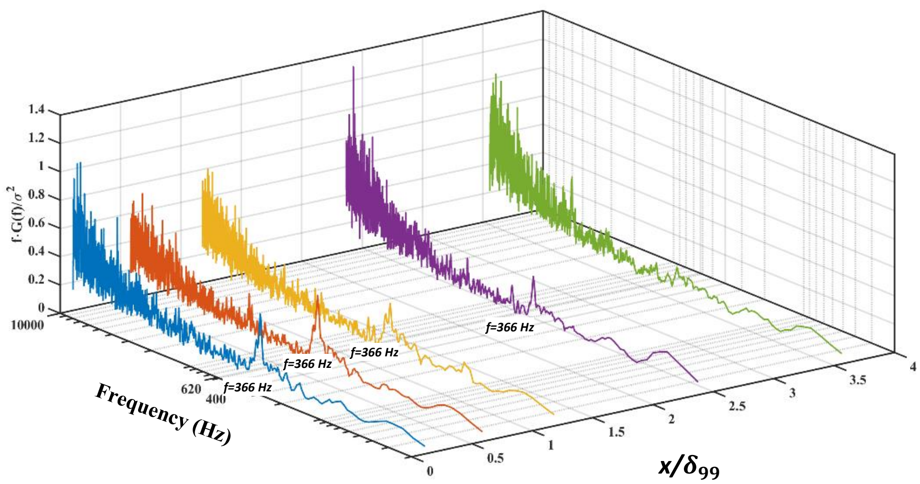

b) Ramp Face

Figure 3 Streamwise Evolution of Premultiplied PSD for the Compliant panel experiments a) Panel Surface b) Ramp Surface (Line Colors used for line identification only)

C. Characterization of the Compliant Panel

In this study, coupling was investigated using the POD technique, which provides spatial characteristics of dominant modes with their time information. The basic equation of the POD decomposition is shown in equation 1. The variable *f* for this study represented pressure or displacement (y-direction). The mean subtracted measured fields were decomposed by spatial-dependent modes ($\phi_i(\boldsymbol{x})$) and corresponding to the time-dependent modes coefficients ($a_i(t)$). $\boldsymbol{x}$ in the equation represents the spatial coordinates, and *i* is the modal index.

$$f(\boldsymbol{x},t) - \overline{f(\boldsymbol{x},t)} = \sum_{i=1}^{n} a_i(t)\phi_i(\boldsymbol{x}) \qquad \text{Equation 1}$$

The structural mode frequencies on a plot and shapes were identified using the mode indicator method and the POD technique, respectively [19]. The mode indicator function [26]is a frequency spectrum that combines information from multiple sensors. The spectral content of a mode depends on the spatial location, thus a single power spectrum could miss out on dominant peaks if the corresponding mode has a node at that location. The mode indicator function circumvents this by including multiple locations in the computation of a single power spectrum. This process is based on first computing the cross-power spectral density matrix between multiple sensors, and then performing a singular value decomposition. It is commonly used in structural dynamics to analyze resonant frequencies.

The mode indicator function is shown in Figure 4, and the plot's peaks showing mode frequencies were identified using POD decomposition. The calculated mode shape $\phi_i(\boldsymbol{x})$ and the peak value of power spectral density (PSD) of the time coefficient provides the frequency information (Figure 5). Relative energy from POD mode decomposition reveals that the first mode energy corresponds to ~96.5%, the second mode energy corresponds to ~2.1%, third and fourth modes are 0.6 and 0.2% of the total energy, respectively.

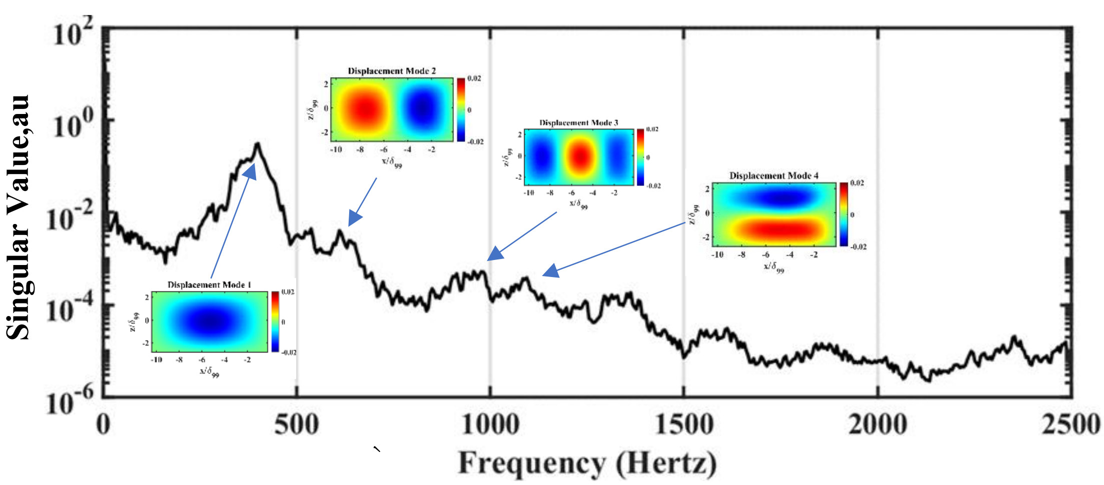

Figure 4 : Mode shapes and associated frequencies of panel deformation from singular value decomposition

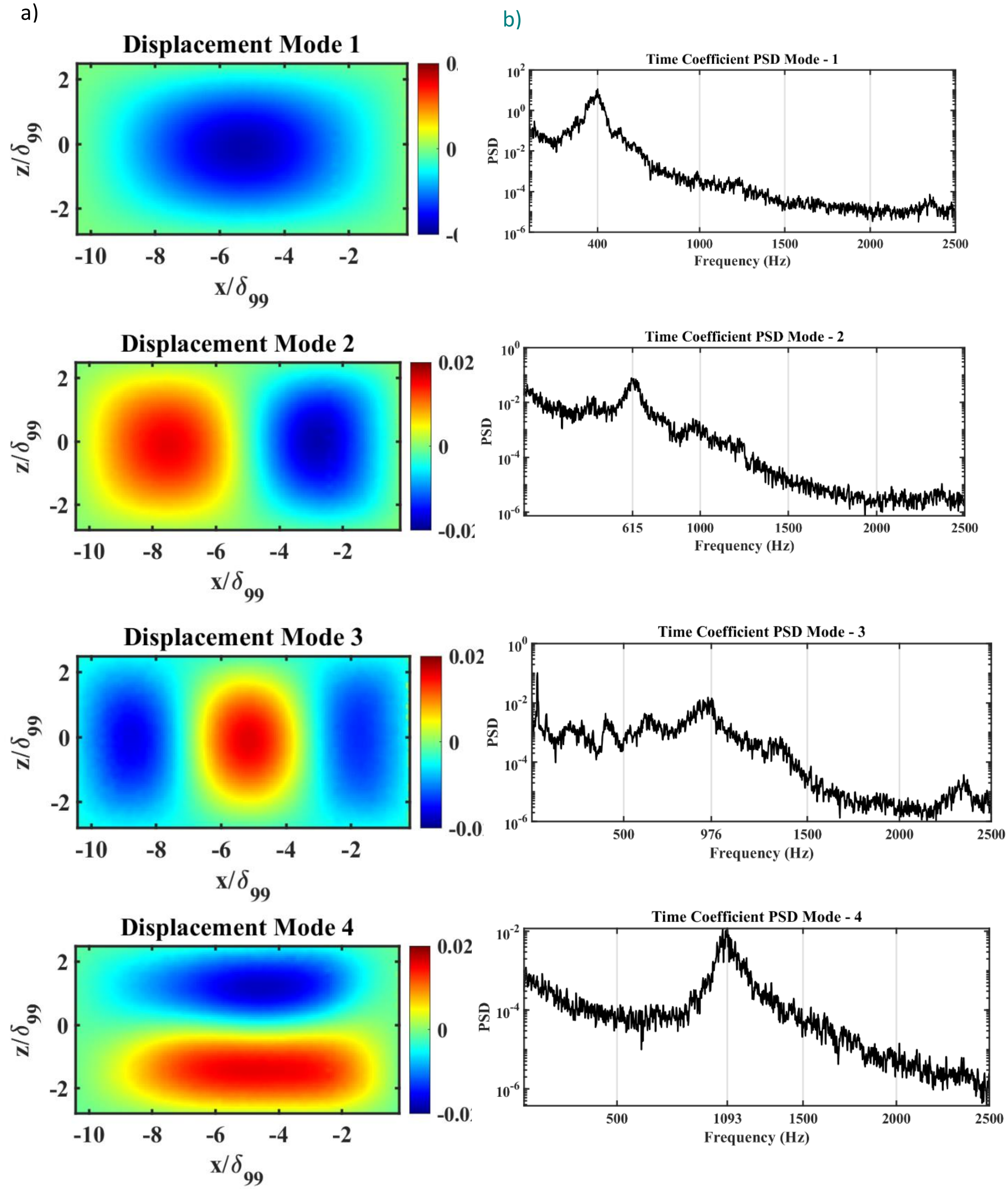

Figure 5 (a) $\phi_i(x)$ of the displacement field from 1-4 modes, and (b) corresponding PSD of time coefficients (a(t))

D. POD of Pressure fields:

POD of the surface pressure fields for the compliant panel was used to investigate potential coupling to the panel dynamics. The same analysis is applied to the rigid panel for comparison purposes. Figure 6 shows the percentage of energy for modes for rigid and compliant panels, and Table 1 shows the percentage of the energy for mode intervals. Figure 6 shows the rigid panel has considerably higher first mode energy, and the second mode energy is similar to the compliant panel case. However, the compliant panel has higher energy for the 3^{rd}-5^{th} modes. Looking at Table 1, the total energy of the first 6 modes of both cases is close to ~60% for two cases, and other modes have comparable values, and the interval shows a 1-2% difference. It can be interpreted that the model energy is distributed between modes for the compliant panel cases.

Figure 7 shows the spectral content of the first 100 modes of pressure time coefficients both for the rigid and compliant panels. It should be noted that the plot is normalized with the standard deviation squared, so darker blue regions show low-level frequency content. The first 100 modes of the spectral range show that as mode number increases, spectral content moves to higher values in the spectrum, which shows that modes at higher mode numbers represent the more turbulent flow. Additionally, energy per mode decreased since smaller-scale structures will be described. In Figure 7, the zoomed-in plot shows that the first 10 -20 modes have lower frequency content. In fact, the frequency content is comparable to the intermittent region frequency content (Figure 3), which is associated with shock foot motion.

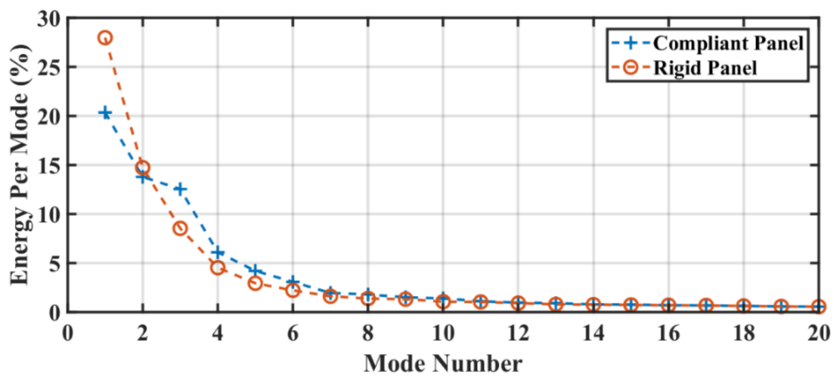

Figure 6 Percentage of Energy Distribution for each modes

Table 1. Cumulative Energy Distribution of Pressure Modes

Modes	Rigid Panel	Compliant Panel
Modes 1-6	60.68%	60.1%
Modes 7-10	5.27%	6.62%
Models 11-20	6.63%	7.5%
Modes 21-100	16.19%	14.25%
Modes 101-2000	10.15%	9.91%

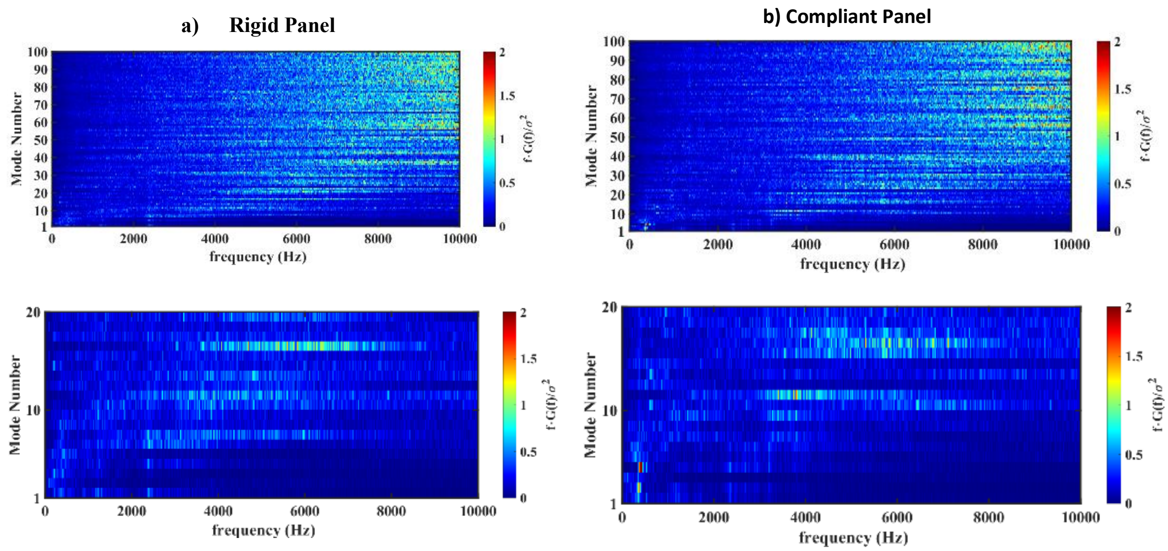

Figure 7 Spectral Content of the first 100 Time Coefficients of Pressure Modes Column a) Rigid Panel b) Compliant Panel

The first 6 mode shapes were chosen to compare due to their higher energy content. Figure 8 shows the first 6 pressure mode shapes of the compliant panel and the rigid panel. Mode 1 of both rigid and compliant panels shows similarities in the blue and red regions on the image. In both mode 1 images, the blue area shows the shock foot oscillation region (intermittent region) and the red region extends from the separation region to the ramp face.
The pressure changes in the separated flow region on the panel and the pressure on the ramp are in phase with each other (since they have the same sign/color). They are however out-of-phase with the pressure changes in the intermitent region, which is the dark blue region around x/δ_{99}=-2. The compliant panel case, upstream of the shock foot, shows yellow and light green regions that were not on the rigid panel, and which could be due to the panel mode effect. Comparing mode 2 for each case shows little similarity. However, it is interesting that some other mode shapes of the compliant panel show similarities with the rigid panel mode shapes. For instance, mode 2 of the rigid panel has a similar shape as the compliant panel mode 3 -- likewise, mode 4 to mode 5, and mode 5 to mode 6.

Pre-multiplied PSD of time POD coefficients of pressure mode comparison was made between the rigid and compliant panels. The comparison was made between the same mode numbers (Figure 9) The first mode comparison shows the spectra are similar except the compliant panel exhibits a high amplitude peak near 390 Hz. Peaks are also observed at 532, 1200, and 2300 Hz. The 2300 Hz peak is a feature that is commonly seen in the tunnel and its origin is not known. No such similar spectral trend was observed for the same mode number comparison of modes 2 to 4. The compliant panel time coefficient shows a peak at a frequency around the fundamental mode frequency of the displacement, and especially Mode 4 shows this at precisely 400 Hz.

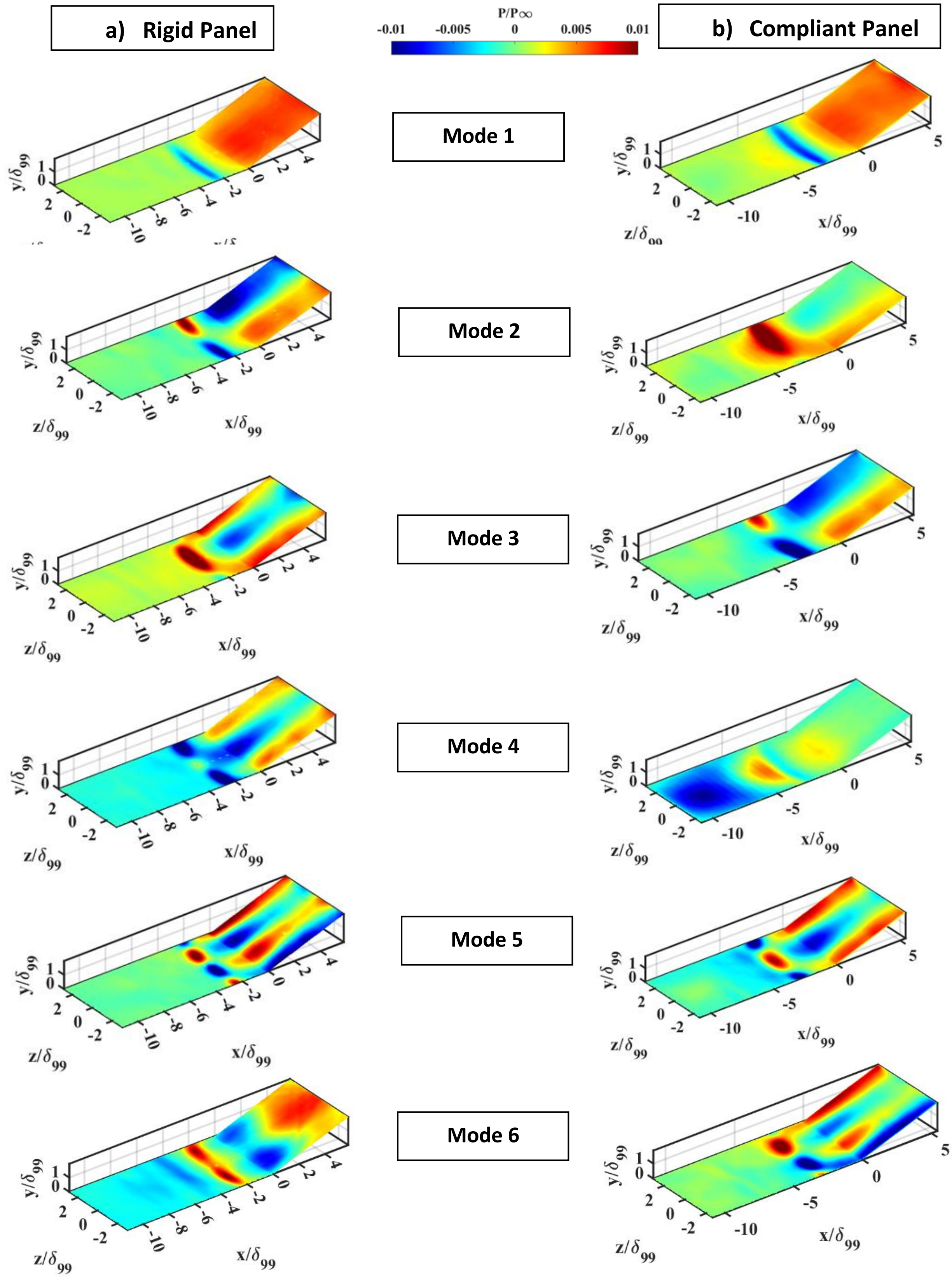

Figure 8 Pressure ratio of the first 6 mode shapes: Column (a): The rigid panel, and (b) The compliant panel

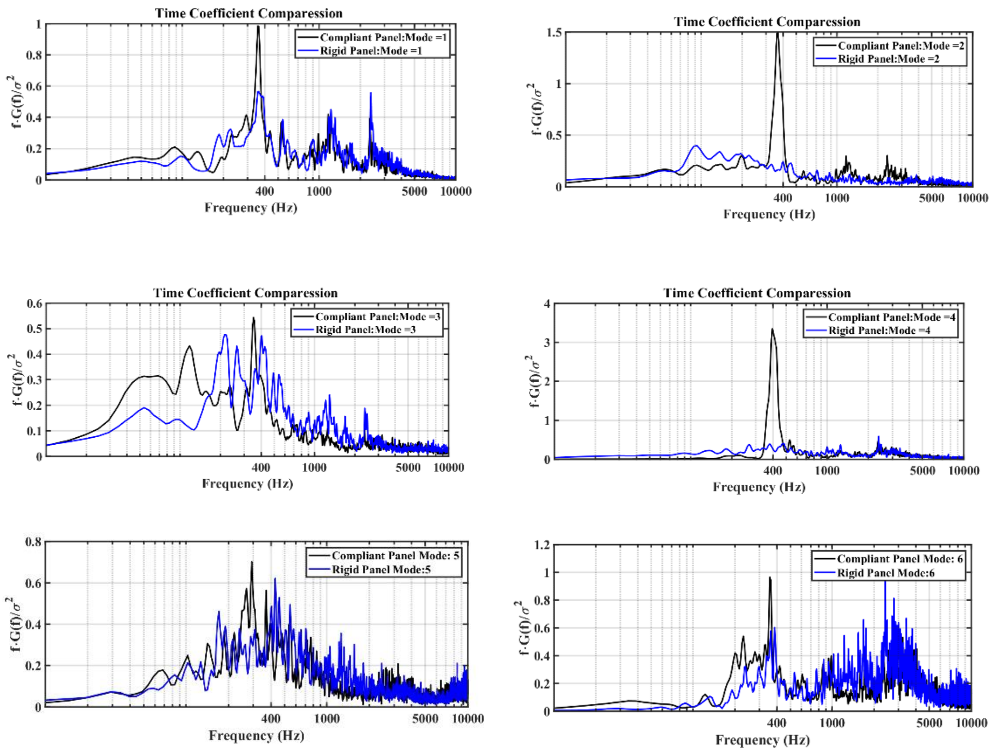

Figure 9 Spectral Comparison of Pressure Mode Time Coefficients of Rigid and Compliant Panel Fields

To investigate the coupling between the modes, a cross-correlation was made between the compliant panel's displacement and pressure time coefficients. The Matlab *xcorr* function was utilized for the calculations. Figure 10 shows the maximum correlation coefficient between the displacement and pressure of the compliant-panel time coefficient of the first 20 modes. The correlations were made for 100 modes, and since 20-100 mode correlations are less than 0.1, are not shown here. For the rigid case, no correlations were measured since there is no displacement measurements. For the compliant panel, Figure 10 shows a correlation coefficient above 0.25. Three coefficients are 0.5 and above; namely, correlations between displacement mode 1 and pressure modes 2 and 4, and between displacement mode 2 and pressure mode 1. The correlation coefficient vs. time lag of those correlations is in Figure 11. All those correlations don't show a time.

The most significant correlation is 0.68, which is between the displacement mode 1 and pressure mode 4. Our previous research shows that the surface displacement gradients (i.e., wall angle) upstream of the shock foot lead to the pressure variation explained by linearized potential flow theory. Considering the streamwise wall angle of displacement mode 1 (Figure 12 a) compared to the upstream pressure mode 4 shape (Figure 4), together with the matched peak frequency of the coefficient of pressure mode 4 as displacement mode 1, seems to explain the correlation. However, as a counterpoint, the other two correlations are not readily explainable using a similar argument. Mode 2 of the pressure field is asymmetric, and the peak frequency (~370 Hz) is close to, but not equal to 400Hz. Similarly, Mode 2 of the wall angle does not match the upstream of the mode 1 shape of the pressure field, and the spectrum of Mode 1 of the pressure field does not show a peak at the same frequency. However, the frequency of the signals is broad-band, which could be the reason that the correlation coefficients are smaller.

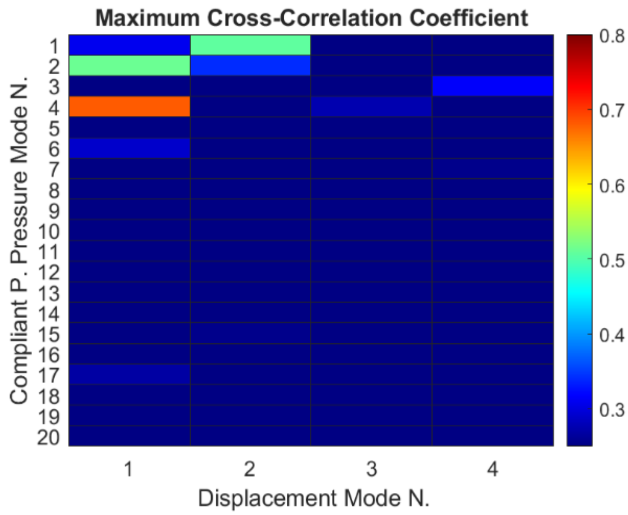

Figure 10 Time Coefficient Correlations between the displacement field and pressure field

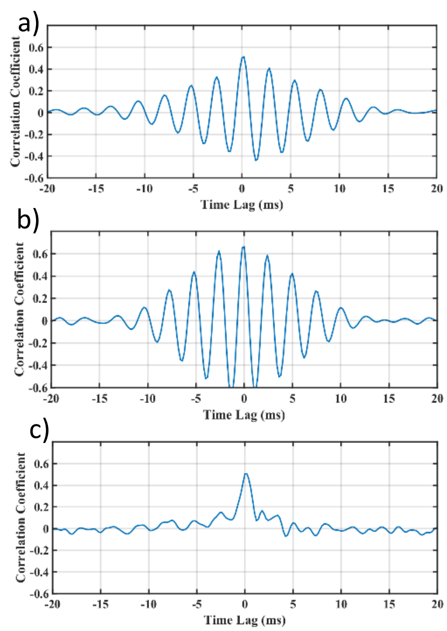

Figure 11 Cross-Correlation between the displacement time coefficient vs compliant panel pressure time coefficient (a) Between Displacement Mode 1 and pressure Mode 2 b) Displacement Mode 1 and Pressure Mode 4 & c) Displacement Mode-2 and Pressure Mode-1.

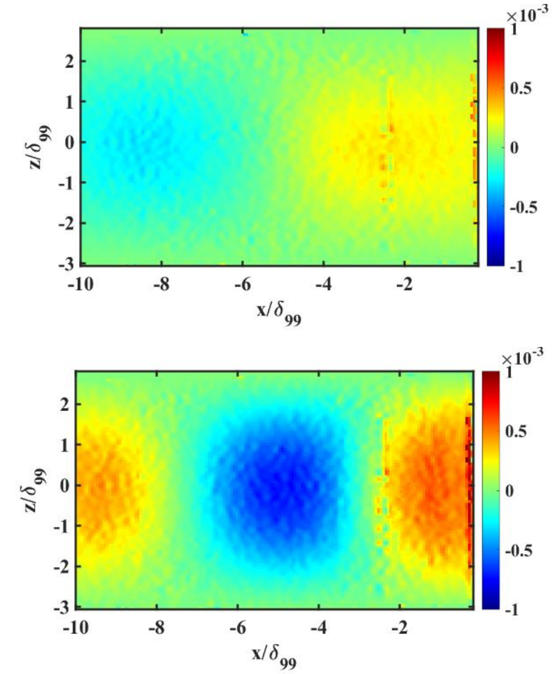

Figure 12 Streamwise gradient of displacement of modes: (Top) Mode 1and (Bottom) Mode 2.

E. Effect of the panel response on Surrogate Shock-foot and reattachment line correlations.

POD analysis shows a reasonably strong correlation between displacement and pressure modes. The correlation is between low-frequency high energy modes, which are the first 4 modes. The low-frequency mode shapes show a connection even on the ramp face, which likely shows panel vibration affects reattachment dynamics. Studies on compression ramp induced SBLI showed that despite the high-frequency content of the flow on the ramp, there is a correlation between the reattachment line and shock foot at low frequencies [27], [28]. Spectral content on the ramp face exhibits low-frequency content associated with the fundamental mode up until x/δ_{99}= 2.5 (Figure 3b).

Shock foot and reattachment line dynamics were investigated by defining surrogate quantities based on pressure threshold values. For the surrogate shock foot, the shock foot was defined as the location where P/P_∞ =1.2 for both compliant and rigid panels, which was based on the pressure gradient change due to the separation shock. For the reattachment line, the correct definition is the line where C_f = 0 [27]–[29]. The local structure was shown on the reattachment pressure line and skin friction line where C_f= 0 by Kavun et al [29].

The region downstream of the reattachment [29] line shows that streamwise periodic structures can be attributed to Gortler-like vortices. Similar observations were observed in the current pressure fields, especially in lowpass (1 kHz) filtered data. For example, for the rigid panel pressure fields, the data shows local fluctuations on the pressure contour (yellow contour) make a 'zigzag' shape (Figure 13). The surrogate shock foot line is roughly the aqua color contour and the reattachment line is the yellow contour. Time sequences of the pressure fields show the movement of these two lines exhibit a kind of breathing motion. Based on the observations, the surrogate reattachment line isobar contour was set to P/P_∞ =1.89 and 1.64 for the rigid panel and the compliant panel cases, respectively. The ratio is lower due to panel deformation on the surface, leading to an increased pressure difference on the ramp.

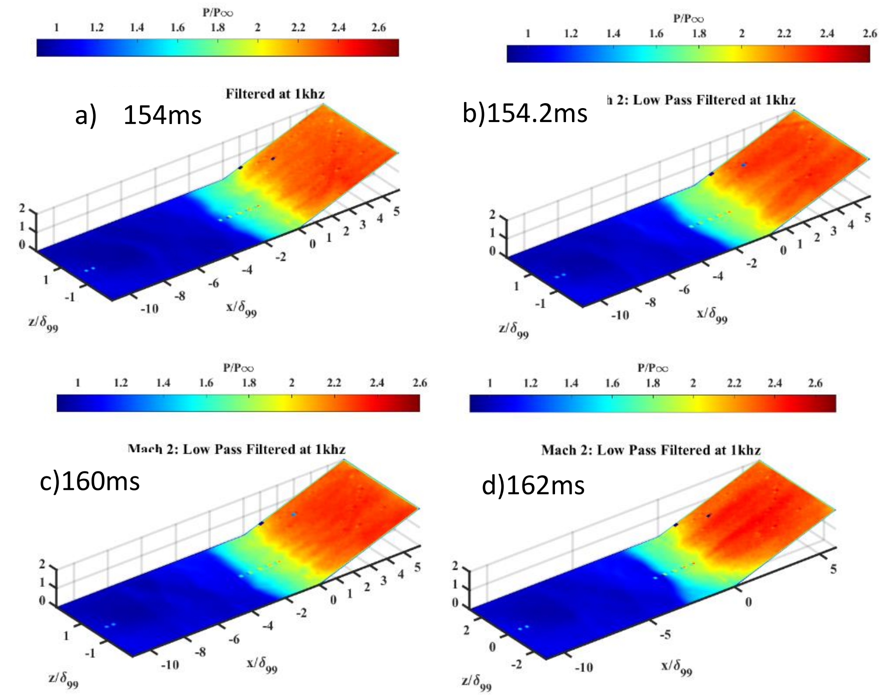

Figure 13 Snapshots from lowpass filtered rigid panel pressure fields

The cross-correlations between separation and reattachment lines were made just off the centerline for the rigid panel to avoid the unpainted Kulite holes, and for the compliant it was on the centerline. Figure 14 shows cross-correlation coefficients for both cases. For the rigid panel, the peak value is seen to be 0.5 with no time lag for the unfiltered data, and a peak value of 0.8 for the lowpass filtered data. On the other hand, for the compliant panel case, the correlation is lower, as it is 0.3 for the unfiltered case and ~0.5 for the lowpass filtered case. For the compliant panel case, there is a time lag of 0.5ms, which means reattachment motion leads shock foot motion. A negative correlation indicates lines approach and move away from the ramp corner at x/δ_{99}= 0, i.e., the separated flow exhibits a breathing motion. The spectral content shows that the compliant panel case, the first mode of the compliant panel effected the shock foot and reattachment line (Figure 3b). Even though it is a low frequency effect, the interaction shows that it lowers the correlation between the reattachment line and shock foot.

To investigate the correlation in frequency domain, the coherence calculations between the shock foot and reattachment lines were made for unfiltered data. The coherence provides the correlation per frequency bins by calculating the magnitude square coherence estimate (Equation 2). Magnitude square coherence estimate is a function of power spectral densities $P_{xx}(f)$, and, $P_{yy}(f)$ and cross-spectral density $P_{xy}(f)$. Coherence vs frequency shows the relation between two signals, and a maximum value of unity represents a linear relation. For this calculation Matlab's 'mschore' function was utilized. Figure 15(a) shows that the coherence has higher values at low frequencies for the rigid panel (<1.5khz), which is expected based on the increase in the cross-correlation coefficient for the low-pass filtered data (Figure 14). Figure 15 also shows that the coherence between separation and reattachment is actually lower for the compliant panel at lower frequecies. The spectrum shows weak peaks near the first two vibration frequencies at 400 Hz and 585 Hz, though they are not dominant.

$$C_{xy} = \frac{|P_{xy}(f)|^2}{P_{xx}(f)P_{yy}(f)} \qquad \text{Equation 2}$$

.

a) Rigid Panel b) Compliant Panel

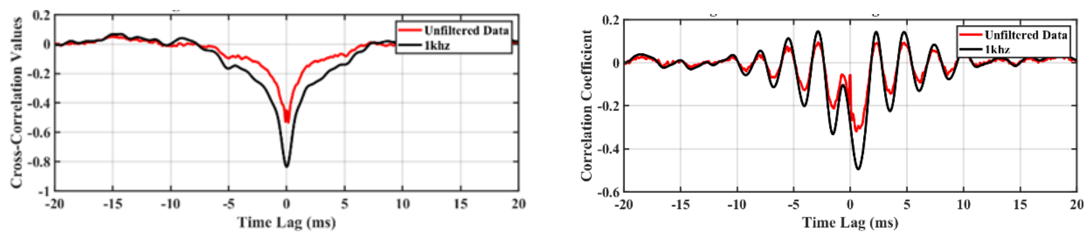

Figure 14 Cross-Correlation between Surrogate Shock-foot and Reattachmen Line: a) Rigid Panel, b) Compliant Panel

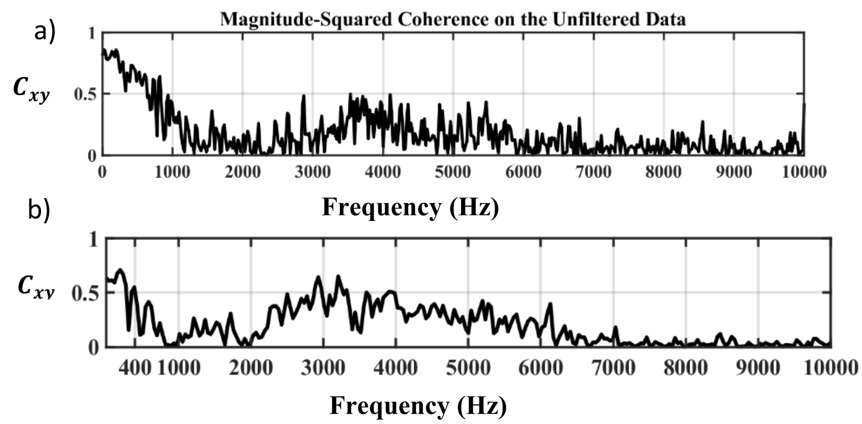

Figure 15 Coherence Estimate between the surrogate shock foot and reattachment lines for: a) Rigid Panel b) Compliant Panel

F. Conclusion and Summary

The simultaneous high-speed pressure and displacement measurements were utilized to investigate the surface pressure unsteadiness on a polycarbonate compliant panel underneath a compression ramp SBLI. The POD technique was used to identify the high energy modes of the pressure field to investigate coupling between the flow and the panel vibration. It was shown that the first six modes contribute sixty percent of energy and have low-frequency content. Although some similarity in the pressure mode shapes exists between the compliant and the rigid panel, the compliant panel pressure mode spectral content shows oscillation at frequencies of panel vibration. The correlations between displacement and pressure modes exist among the lower-ranked modes. The highest correlation was between displacement mode 1 and pressure mode 4, which can be explained by linearized potential flow relations upstream of the flow separation.

Further studies were made between the surrogate shock foot and the reattachment line. The panel vibration lowers the surrogate shock-foot and reattachment line correlation at a lower frequency. A more detailed study will be required on the reason for this correlation as a future work which will include the velocity measurements for detailed interaction analysis.

G. Acknowledgments

This work was supported by the National Science Foundation under award # 1913587.

References

[1] D. S. Dolling, “Fifty Years of Shock-Wave/Boundary-Layer Interaction Research: What Next?,” *AIAA Journal*, vol. 39, no. 8, pp. 1517–1531, Aug. 2001, doi: 10.2514/2.1476.

[2] N. T. Clemens and V. Narayanaswamy, “Low-Frequency Unsteadiness of Shock Wave/Turbulent Boundary Layer Interactions,” *Annual Review of Fluid Mechanics*, vol. 46, no. 1, pp. 469–492, Jan. 2014, doi: 10.1146/annurev-fluid-010313-141346.

[3] J. J. McNamara and P. P. Friedmann, “Aeroelastic and Aerothermoelastic Analysis in Hypersonic Flow: Past, Present, and Future,” *AIAA Journal*, vol. 49, no. 6, pp. 1089–1122, 2011, doi: 10.2514/1.J050882.

[4] S. Willems, A. Gülhan, and B. Esser, “Shock induced fluid-structure interaction on a flexible wall in supersonic turbulent flow,” vol. 5, pp. 285–308, 2013, doi: 10.1051/eucass/201305285.

[5] L. Maestrello and T. L. J. Linden, “Measurements of the response of a panel excited by shock boundary-layer interaction,” *Journal of Sound and Vibration*, vol. 16, no. 3, pp. 385–388, 1971, doi: 10.1016/0022-460X(71)90594-3.

[6] S. M. Spottswood, T. Eason, and T. Beberniss, “Full-field, dynamic pressure and displacement measurements of a panel excited by shock boundary-layer interaction,” May 2013. doi: 10.2514/6.2013-2016.

[7] S. M. Spottswood *et al.*, “Exploring the response of a thin, flexible panel to shock-turbulent boundary-layer interactions,” *Journal of Sound and Vibration*, vol. 443, pp. 74–89, 2019, doi: 10.1016/j.jsv.2018.11.035.

[8] S. M. Spottswood, T. Eason, and T. Beberniss, “Influence of shock-boundary layer interactions on the dynamic response of a flexible panel,” *Proceedings of the International Conference on Noise and Vibration Engineering ISMA 2012*, pp. 603–616, 2012.

[9] S. v. Varigonda, C. Jenquin, and V. Narayanaswamy, “Impact of Panel Vibrations on the Dynamic Field Properties in Supersonic ow,” 2021. doi: 10.2514/6.2021-2926.

[10] S. Willems, A. Gülhan, and B. Esser, “Shock induced fluid-structure interaction on a flexible wall in supersonic turbulent flow,” vol. 5, pp. 285–308, 2013, doi: 10.1051/eucass/201305285.

[11] M. C. Neet and J. M. Austin, “Effects of surface compliance on shock boundary layer interactions in the caltech mach 4 ludwieg tube,” in *AIAA Scitech 2020 Forum*, 2020, vol. 1 PartF. doi: 10.2514/6.2020-0816.

[12] M. A. Eitner, Y. J. Ahn, M. N. Musta, N. T. Clemens, and J. Sirohi, “Effect of Structural Modifications on Vibratory Response of a Panel under Ramp-Induced Shock / Boundary Layer Interaction,” AIAA Scitech 2486-2022. doi: 10.2514/6.2022-2486.

[13] Y. J. Ahn, M. Musta, M. Eitner, J. Sirohi, and N. Clemens, “ Experimental Investigation of Flow-Structure Interaction for a Compliant Panel under a Mach 2 Compression-Ramp”, AIAA SciTech Forum 0293-2022. doi: 10.2514/6.2022-0293.c1.

[14] M. Eitner, M. Musta, L. Vanstone, J. Sirohi, and N. Clemens, “Modal Parameter Estimation of a Compliant Panel Using Phase-based Motion Magnification and Stereoscopic Digital Image Correlation,” *Experimental Techniques*, pp. 287–296, 2020, doi: 10.1007/s40799-020-00393-6.

[15] T. J. Goller, D. U. Mustafa N. Musta, Leon Vanstone, and N. T. C. Lee Mears, Jayant Sirohi, “Simultaneous High-Speed Displacement and Surface Pressure Measurements of a Compliant Panel under a Mach 2 Compression Ramp Interaction,” *Presented in AIAA SciTech*, 2019.

[16] T. J. Goller, M. N. Musta, D. Uehara, & Sirohi, J., and N. Clemens, “Experimental Study of a Compliant Panel under a Mach 2 Compression Ramp Interaction,” , *71st Annual Meeting of the APS Division of Fluid Dynamics*, 2018.

[17] M. Musta, L. Vanstone, M. Eitner, J. Sirohi, and N. T. Clemens, “A Compression - Ramp Shock/Boundary-Layer Interaction Over a Compliant Panel at Mach 5,” *72nd Annual Meeting of the APS Division of Fluid Dynamics*, 2019.

[18] T. J. Goller, “Simultaneous High-Speed Displacement and Surface Pressure Measurements of a Compliant Panel under a Mach 2 Compression Ramp Interaction,” MSc. Thesis, University of Texas at Austin, 2019. doi: http://dx.doi.org/10.26153/tsw/2151.

[19] M. A. Eitner, Y. J. Ahn, M. N. Musta, L. Vanstone, J. Sirohi, and N. T. Clemens, “Effect of Shock Wave Boundary Layer Interaction on Vibratory Response of a Compliant Panel,” *AIAA Aviation 2493-2021*. doi: 10.2514/6.2021-2493.

[20] M. N. Musta, Y. J. Ahn, M. A. Eitner, J. Sirohi, and N. T. Clemens, “Investigation of flow-structure coupling for a compliant panel under a shock / boundary-layer interaction using fast- response PSP,”, *AIAA Aviation 2809-2021*, doi: 10.2514/6.2021-2809.

[21] B. Ganapathisubramani, “Statistical properties of streamwise velocity in a supersonic turbulent boundary layer,” *Physics of Fluids*, vol. 19, no. 9, p. 098108, 2007, doi: 10.1063/1.2772303.

[22] L. Vanstone, M. N. Musta, S. Seckin, and N. Clemens, “Experimental study of the mean structure and quasi-conical scaling of a swept-compression-ramp interaction at Mach 2,” *Journal of Fluid Mechanics*, vol. 841, pp. 1–27, Apr. 2018, doi: 10.1017/jfm.2018.8.

[23] R. D. Blevins and R. Plunkett, *Formulas for Natural Frequency and Mode Shape*, vol. 47, no. 2. New York: Van Nostrand Reinhold Co., 2009. doi: 10.1115/1.3153712.

[24] A. J. Wheeler and A. R. Ganji, *Introduction to Engineering Experimentation*, 2nd ed. New Jersey, New York: Prentice Hall, 1996.

[25] Y. Egami, Y. Hasegawa, Y. Matsuda, T. Ikami, and H. Nagai, “Ruthenium-based fast-responding pressure-sensitive paint for measuring small pressure fluctuation in low-speed flow field,” *Measurement Science and Technology*, vol. 32, no. 2, 2021, doi: 10.1088/1361-6501/abb916.

[26] R. Brinker, L. Zhang , and P. Anderson, “Modal Identification from ambient responses using frequency domain decomposition,” *18th International Modal Analysis Conference IMAC*, San Antonio,TX, 2000.

[27] S. Priebe and M. P. Martín, “Low-frequency unsteadiness in shock wave–turbulent boundary layer interaction,” *Journal of Fluid Mechanics*, vol. 699, pp. 1–49, 2012, doi: 10.1017/jfm.2011.560.

[28] M. Wu and M. P. Martin, “Direct Numerical Simulation of Supersonic Turbulent Boundary Layer over a Compression Ramp,” *AIAA Journal*, vol. 45, no. 4, pp. 879–889, 2007, doi: 10.2514/1.27021.

[29] I. N. Kavun, I. I. Lipatov, and V. I. Zapryagaev, “International Journal of Heat and Mass Transfer Flow effects in the reattachment region of supersonic laminar separated flow,” *International Journal of Heat and Mass Transfer*, vol. 129, pp. 997–1009, 2019, doi: 10.1016/j.ijheatmasstransfer.2018.09.125.